Physiological Origin of Low-Frequency Drift in Blood Oxygen Level Dependent (BOLD) Functional Magnetic Resonance Imaging (fMRI)

Lirong Yan,[1,2] Yan Zhuo,[1,3*] Yongquan Ye,[1,2] Sharon X. Xie,[5] Jing An,[3,4] Geoffrey K. Aguirre,[6] and Jiongjiong Wang[6,7*]

We investigated the biophysical mechanism of low-frequency drift in blood-oxygen-level-dependent (BOLD) functional magnetic resonance imaging (fMRI) (0.00–0.01 Hz), by exploring its spatial distribution, dependence on imaging parameters, and relationship with task-induced brain activation. Cardiac and respiratory signals were concurrently recorded during MRI scanning and subsequently removed from MRI data. It was found that the spatial distribution of low-frequency drifts in human brain followed a tissue-specific pattern, with greater drift magnitude in the gray matter than in white matter. In gray matter, the dependence of drift magnitudes on TE was similar to that of task-induced BOLD signal changes, i.e., the absolute drift magnitude reached the maximum when TE approached T_2^* whereas relative drift magnitude increased linearly with TE. By systematically varying the flip angle, it was found that drift magnitudes possessed a positive dependence on image intensity. In phantom experiments, the observed drift was not only much smaller than that of human brain, but also showed different dependence on TE and flip angle. In fMRI studies with visual stimulation, a strong positive correlation between drift effects at baseline and task-induced BOLD signal changes was observed both across subjects and across activated pixels within individual participants. We further demonstrated that intrinsic, physiological drift effects are a major component of the spontaneous fluctuations of BOLD fMRI signal within the frequency range of 0.0–0.1 Hz. Our study supports brain physiology, as opposed to scanner instabilities or cardiac/respiratory pulsations, as the main source of low-frequency drifts in BOLD fMRI. Magn Reson Med 61:819–827, 2009. © 2009 Wiley-Liss, Inc.

Low-frequency fluctuation or drift is commonly observed in functional magnetic resonance imaging (fMRI) data acquired using blood-oxygen-level-dependent (BOLD) contrast (1). Drift effects, manifested as elevated power at the lower end of the frequency spectrum (generally defined as <0.01 Hz), is an important factor affecting the reliability and accuracy of, as well as suitable experimental design for, BOLD fMRI. Considerable research has been devoted to modeling and thereby removing drift effects in statistical analyses of BOLD fMRI data using linear, lower-order polynomial fitting and high-pass temporal filtering (1–3). Drifts have been further characterized using the 1/frequency (1/f) (4) and higher-order autocorrelation functions (5,6), which could be incorporated subsequently into general linear model (GLM) analyses to account for associated confounding effects (1,2). Although generally successful, these approaches may inordinately reduce the effective degree of freedom of statistical analyses, and may limit the use of low-frequency task designs (long epochs of experimental conditions) in BOLD fMRI studies (7,8).

Paralleling these undertakings from the signal processing perspective have been studies aimed at understanding the biophysical mechanisms underlying low-frequency drifts in BOLD fMRI. To date there has been no consensus as to their source. Earlier studies showed that drifts are mainly attributed to scanner instabilities, which can be observed with inert phantoms as well as human subjects (4,9). Other evidence suggested that low-frequency fluctuations or baseline drift effects may reflect spontaneous neuronal events arising from fluctuations in metabolic-linked brain physiology (10–15). For instance, Hyde et al. (10) reported a positive linear relationship between low-frequency fluctuations (0.0–0.1 Hz) and task-induced BOLD signal changes across activated brain pixels, suggesting that low-frequency noise and BOLD fMRI signals share a metabolic and physiologic source. Such metabolic-linked physiological noise in BOLD fMRI has been modeled based on its unique dependence on the echo-time (TE) and image intensity, with the noise magnitude reaching its peak when TE approximates the apparent transversal relaxation time (T_2^*) (16). More recently, there has been evidence suggesting that respiratory and cardiac pulsation effects contribute to the enhanced low-frequency noise in BOLD fMRI through aliasing or variations in cardiac and respiratory rate (12,17–20). It was further suggested that cardiac-induced fluctuations may be spatially focal (21,22)

[1]State Key Laboratory of Brain and Cognitive Science, Institute of Biophysics, Chinese Academy of Sciences, Beijing, China.

[2]Graduate School, Chinese Academy of Sciences, Beijing, China.

[3]Beijing MRI Center for Brain Research, Beijing, China.

[4]Siemens Mindit Magnetic Resonance Ltd., Shenzhen, China.

[5]Department of Biostatistics and Epidemiology, University of Pennsylvania, Philadelphia, Pennsylvania, USA.

[6]Department of Neurology, University of Pennsylvania, Philadelphia, Pennsylvania, USA.

[7]Department of Radiology, University of Pennsylvania, Philadelphia, Pennsylvania, USA.

*Correspondence to: Jiongjiong Wang, Ph.D., Department of Radiology, University of Pennsylvania, 3400 Spruce Street, Philadelphia, PA 19104. E-mail: wangj3@mail.med.upenn.edu; or Y.Z., State Key Laboratory of Brain & Cognitive Science, Institute of Biophysics, Chinese Academy of Sciences, 15 Datun Road, Beijing 100101, China. E-mail: yzhuo@bcslab.ibp.ac.cn

and exhibit TE dependence (23), whereas the respiration-induced noise may be more globally distributed (19,22) and largely TE independent (23). In summary, three main sources of drift effects have been proposed in past studies, namely: 1) scanner instability; 2) spontaneous fluctuation in brain metabolism and physiology; and 3) physiologic noise from systemic sources such as cardiac and respiratory cycles.

The primary purpose of the present study was to identify which of these three possible sources contribute to low-frequency (here considered to be 0.00–0.01 Hz) signal drift in BOLD fMRI. We addressed this issue by systematically comparing drift effects measured from human participants and an agarose gel phantom. Cardiac and respiratory signals were concurrently recorded during human scans and subsequently removed from MRI data. A secondary goal of the present study was to address the relationship between drift effects (0.00–0.01 Hz) and low-frequency physiological noise (0.0–0.1 Hz) commonly used in "resting state" BOLD fMRI studies (24).

MATERIALS AND METHODS

All studies were performed on a Siemens 3T TIM Trio whole-body MR system (Siemens, Erlangen, Germany). A total of 15 healthy volunteers (mean ± standard deviation [SD] age = 26.5 ± 7.0 years, 10 males) participated in this study after they provided written informed consent, according to a protocol approved by the Institutional Review Board. The fMRI study consisted of three main experiments: resting state with varying TE; task activation with varying TE; and resting state with varying flip angle.

Resting State Experiment With Varying TE

A single-shot dual-echo gradient-echo echo planar imaging (EPI) sequence with interleaved TE was developed to acquire four different TE data sets for every two consecutive TRs (TE1 = 20 ms and TE2 = 50 ms for one TR, TE3 = 35 ms and TE4 = 65 ms for the following TR). The interleaved TE provided an effective means to control the confounding effect of temporal changes in experimental condition irrelevant to the variable of interest (e.g., TE). Two values of TR were used in this study: 1) TR = 1 s or effective TR = 2 s, corresponding to a temporal resolution comparable to those routinely used for fMRI studies. Ten oblique slices with thickness = 5 mm and gap = 1 mm were scanned, with the slices parallel to the anterior–posterior commissure (AC-PC); 2) TR = 125 ms or effective TR = 250 ms, which was chosen to eliminate or minimize aliasing effects from respiratory and cardiac pulsations (11,12,20). A single oblique slice of 5 mm (parallel to AC-PC) was scanned through the Calcarine fissure. Other imaging parameters were: FOV = 24 cm, matrix size = 64 × 64, bandwidth = 2442 Hz/pixel, flip angle = 65° for TR of 1 s, and 25° for TR of 125 ms.

Seven healthy volunteers (age 23.4 ± 1.7 years, four males) were scanned using the product's 12-channel head coil. Each participant underwent two scans (8 min each) during resting state using the dual-echo EPI sequence with interleaved TE for the two TR conditions, respectively. During the resting state, subjects were instructed to close their eyes, rest quietly, and avoid any particular cognitive activity. For each subject, conventional T_1-weighted three-dimensional (3D) images were acquired using an magnetization-prepared rapid gradient-echo (MPRAGE) sequence (TR/TE/TI = 1730 ms/3.96 ms/1100 ms, flip angle = 15°, matrix size = 128 × 128, voxel size = 1.9 × 1.9 × 1.9 mm³, acquisition time = 3 min 43 s) for anatomic MRI.

Task Activation Experiment with Varying TE

The seven participants also underwent an 8-min task activation scan following the resting scans described above during the same MRI session. The same dual-echo EPI sequence with four interleaved TEs was used, and imaging parameters were identical to the resting scan of TR = 1 s. A block design was employed for task activation studies, which consisted of visual stimulation with 10-Hz flashing checkerboard. A sequential 30-s OFF/ON paradigm (eight cycles) was applied as the stimulation during the activation scan. During both resting and task activation scans, cardiac and respiratory signals were recorded using the scanner's built-in photoplethysmograph and a respiratory belt, respectively. To identify the cardiac and respiratory phases in which images were acquired, the transistor-transistor logic (TTL) pulse converted from the optical trigger signal generated by the Siemens scanner was recorded for each measurement after it was prolonged to 10 ms using a custom-built circuit.

Resting State Experiment With Varying Flip Angle

To investigate the relationship between low-frequency drift and image intensity, we modulated the MR image intensity by systematically varying the flip angle. Eight subjects (age 29.2 ± 8.7 years, six males) were scanned using the standard transmit/receive (Tx/Rx) head coil, and underwent MRI scanning using a standard single-shot gradient-echo EPI sequence with four different flip angles (30°/45°/60°/75°). Each scan with a fixed flip angle took 4 min (120 acquisitions), and a single TE of 35 ms was applied for all four scans. The rest imaging parameters were: FOV = 22 cm, matrix size = 64 × 64, TR = 2 s, 20 × 5-mm slices gapped by 1 mm, bandwidth = 2442 Hz/pixel.

The experiments described above (dual-echo EPI with interleaved TE and varying flip angle) were also performed on a cylindrical gel phantom (10-cm diameter) made of 2% agarose doped by 0.45 mM/liter CuSO$_4$ (25). This gel agarose phantom was designed to simulate the physiological properties of human brain, with T_1 and T_2 values of 1159 ± 30 ms and 80.3 ± 0.5 ms, respectively.

Data Processing

All EPI data were corrected for head motion offline using SPM2 (Wellcome Department of Imaging Neuroscience, University College London, UK), which was performed independently for each TE of each measurement. For subjects participating in both resting state and task activation experiments, image registration was also performed to align the resting and activation scans. No spatial smoothing was applied since previous studies have shown that spatial smoothing may modulate (enhance) the magnitude of low-frequency noise in BOLD fMRI (26,27).

For retrospective correction of respiratory and cardiac pulsations, we followed the standard procedure according to retrospective image-based correction (RETROICOR) (28). Cardiac phase was calculated assuming it linearly advanced from 0 to 2π between two adjacent peak pulse signals, whereas a histogram-equalized transfer function between respiratory amplitude and phases was applied to determine the respiratory phase. BOLD signals related to cardiac and respiratory pulsations were estimated and then removed for each pixel, based on a second-order Fourier series using a program developed in-house (28).

To quantify the magnitude of low-frequency drift, previous studies have used the total power of the low-frequency band (0.00−0.01 Hz) in the power spectrum of the fMRI time series (9). Other studies relied on the calculation of the SD of the fMRI time series to quantify the magnitude of physiological noise (10,16). In the present study, the absolute magnitude of low-frequency drift, M_{abs}, was determined by

$$M_{abs} = \frac{2}{\sqrt{2}N} \sqrt{\sum_{k=t}^{K} |X(k)|^2} \qquad [1]$$

where $X(k)$ is the discrete Fourier transform of the fMRI time series with N images, and K is the number of the frequency components in the low-frequency band (excluding the term at zero frequency). Since the magnitude of the discrete Fourier transform of the fMRI time series at each frequency (except zero frequency) equals $N/\sqrt{2}$ times the SD of signal at that frequency, M_{abs} is equivalent to the SD of the low-frequency drift, which has been verified empirically. To account for the effect of variations in raw image intensity, relative drift magnitude, M_{rel}, was calculated by scaling M_{abs} as reference to the mean intensity of the corresponding raw EPI time series (expressed as a percentage).

Both absolute and relative magnitudes of low-frequency drift were calculated in each pixel for fMRI data acquired during the resting state. In each individual subject, the mean drift magnitudes were averaged in the whole brain and three regions-of-interest (ROI) of gray/white matter and cerebrospinal fluid (CSF). The gray (voxel count = 5399 ± 684) and white matter (voxel count = 2756 ± 331) ROIs were automatically segmented from the calculated T_2^* maps using SPM2. For CSF, to avoid partial volume effects on the edge of the brain, we manually chose pixels within the lateral ventricles (voxel count = 136 ± 70) as the ROI. The maps of absolute and relative drift magnitudes were coregistered with the anatomical MRI of individual subjects and then normalized into a canonical space (Montreal Neurological Institute standard brain). Normalized maps of drift magnitudes were further averaged across subjects to demonstrate the mean spatial distribution of low-frequency drifts in BOLD fMRI.

Task activation data were analyzed using GLM in SPM2. Spatial smoothing using an "optimum" Gaussian kernel of full-width at half-maximum (FWHM) 6/6/8 mm, and high-pass temporal filtering (Gaussian-weighted least squares fit (LSF) straight line fitting, with σ = 128 s) were applied in preprocessing. The Z statistic maps were thresholded at a
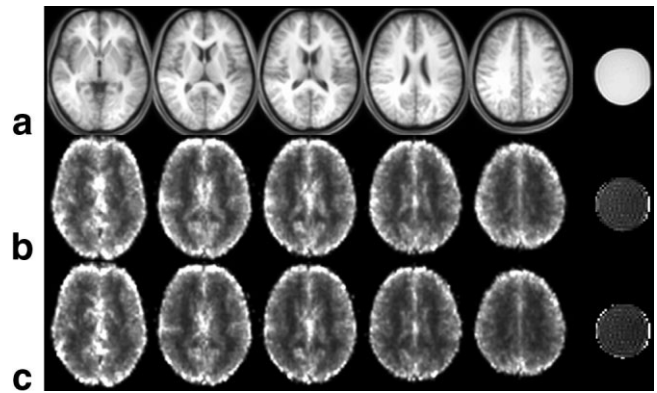

FIG. 1. Mean spatial distribution of low-frequency drifts in seven human subjects and agarose phantom. The average normalized T_1-weighted structural image (**a**), and spatial distribution of the average absolute (**b**) and relative (**c**) magnitude of low-frequency drift are shown in five representative slices.

significance level of $P < 10^{-7}$ with at least 20 contiguous voxels for each TE dataset in each subject. Task-induced signal changes were calculated within ROIs of activated clusters in the visual cortex, and were compared to the baseline drift data within the same ROI. The ROI was defined by the pixels demonstrating common activation for all TE data in the visual cortex. Within the visual area ROI, voxel-based analyses were performed to investigate the relationship between task-induced BOLD signal changes and drift magnitudes at baseline across pixels. For this voxel-based analysis, to avoid the effect of spatial smoothing, measures of BOLD signal changes and drift magnitudes were derived from unsmoothed data in each activated brain pixel. In addition, quantitative T_2^* maps were generated based on a monoexponential model (29).

Statistical analyses were performed using the SPSS 12.0 software package (SPSS, Inc., Chicago, IL, USA). The two-tailed repeated measures analysis of variance (ANOVA) was applied to test the effect of TE and flip angle on drift magnitudes. Pearson correlation coefficients were used to evaluate associations between drift magnitudes and BOLD signal changes.

RESULTS

Spatial Distribution of Low-Frequency Drift

Figure 1 displays the mean spatial distribution of low-frequency drifts after retrospective correction of cardiac and respiratory noise in BOLD fMRI averaged across seven healthy subjects. Data were acquired using the dual-echo EPI sequence with interleaved TE and the representative dataset with TE = 35 ms are shown in five axial sections in Fig. 1. The greatest drift effects seemed to be distributed along the edge of the brain. In the brain parenchyma, drift effects showed relatively uniform spatial distribution, with greater amplitude in gray matter compared to white matter. Statistical analyses of ROI-based measures showed that, at each TE, both the absolute and relative magnitude of low-frequency drifts were significantly greater in gray matter than in white matter ($P < 0.01$). The mean ratio of drift magnitudes averaged across four TEs in CSF (inside
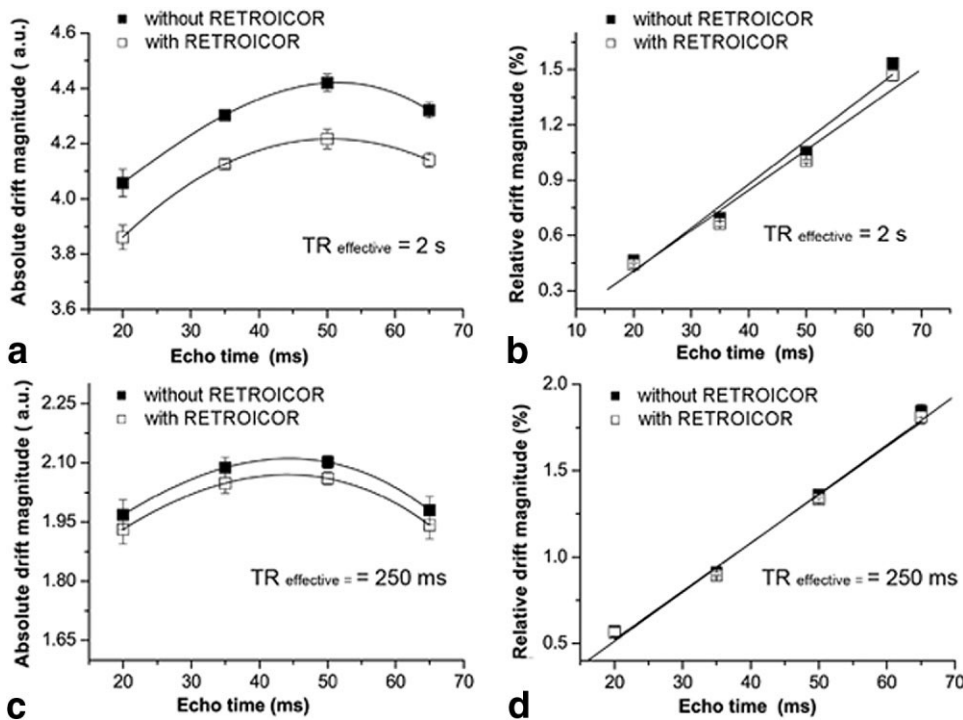
FIG. 2. Mean absolute (**a,c**) and relative magnitude (**b,d**) of low-frequency drifts as a function of TE acquired in seven human subjects. Both data before and after RETROICOR of cardiac and respiratory effects are shown. Best fitted curves are presented on the graphs for absolute drift magnitudes, and linear fitting is performed on relative drift magnitudes. Error bars ($\pm$ SEM) represent the variability across subjects. Whole brain data acquired with an effective TR of 2 s are shown in (a) and (b), data acquired with an effective TR of 250 ms are shown in (c) and (d).

lateral ventricles), gray and white matter was 2.2:1.9:1 and 1.6:2.4:1 for absolute and relative measures, respectively. The last column of Fig. 1 shows the distribution of slow drifts in the agarose phantom, which is uniform except for the edges.

Dependence of Low-Frequency Drift on Echo Time

Figure 2 shows the mean absolute and relative magnitude of low-frequency drift as a function of TE in whole brain (including gray matter, white matter, and CSF ROIs) averaged across seven subjects in the two TR conditions. It can be seen that, with or without correction of respiration and cardiac effects, the absolute magnitude of low-frequency drift reached the maximum when TE approximated the T_2^* of human brain ($T_2^* = 51.85 \pm 3.11$ ms) ($P < 0.001$), and the relative drift magnitude increased linearly with TE ($P < 0.001$). We also observed that the contribution of respiratory and cardiac fluctuations to low-frequency drift was not significantly affected by TE ($P = 0.57$). Figure 3 displays the results based on segmented ROIs of gray matter, white matter, and CSF. The relationship between drift and TE in the gray matter ROI (see Fig. 3a: $T_2^* = 49.50 \pm 2.16$ ms, $P < 0.001$) was consistent with that of the whole brain. Due to the relatively long T_2^* in CSF ($T_2^* = 92.84 \pm 18.39$ ms), the absolute drift magnitude was expected to increase within the range of the four TEs employed in our study. Our empirical data from the CSF ROI was very consistent with the theoretical prediction. However, in the white matter ROI ($T_2^* = 52.30 \pm 1.78$ ms), the absolute drift magnitude showed a trend of decreasing intensity with TE. This finding was similar to that observed in the agarose phantom and will be discussed below. In our experiment, the mean values of T_2^* in the whole brain, gray matter, white matter, and CSF ROIs were generated using a mono-

exponential model (29), which agreed well with literature values (16,30–32).

The relationship between low-frequency drift and TE in the agarose gel phantom is shown in Fig. 4. Data were acquired using the dual-echo EPI sequence with interleaved TE. The absolute magnitude of low-frequency drift in the agarose phantom ($T_2^* = 56.8 \pm 1.2$ ms) decreased with increasing TE ($P < 0.01$). The mean relative magnitude of low-frequency drift was much smaller in the phantom than that of the human brain (approximately 1:4). Furthermore, the change of relative drift magnitude across TE was much smaller than that of human data, although the effect of TE was still significant ($P < 0.01$).

These data suggest that drift effects in the human brain follow a tissue specific pattern. In particular, drifts in gray matter demonstrate a characteristic pattern with absolute drift magnitude peaking when TE approximates T_2^*. In contrast, this relationship was absent in phantom data and in human white matter.

Relationship Between Low-Frequency Drift and BOLD fMRI Signal Change

For clarity, we report in this section results based on relative drift magnitude and fractional BOLD signal changes in response to task activation, since the corresponding absolute measures yielded similar results with a less significant P-value. Figure 5a shows scatter plots of the mean relative drift magnitude at baseline vs. the mean fractional BOLD signal change during activation in visual cortex ROI at four different TEs in the seven subjects. We found strong positive correlation between BOLD signal changes during task activation and low-frequency drifts at baseline in visual ROIs across the seven subjects (r = 0.79, $P < 0.001$).
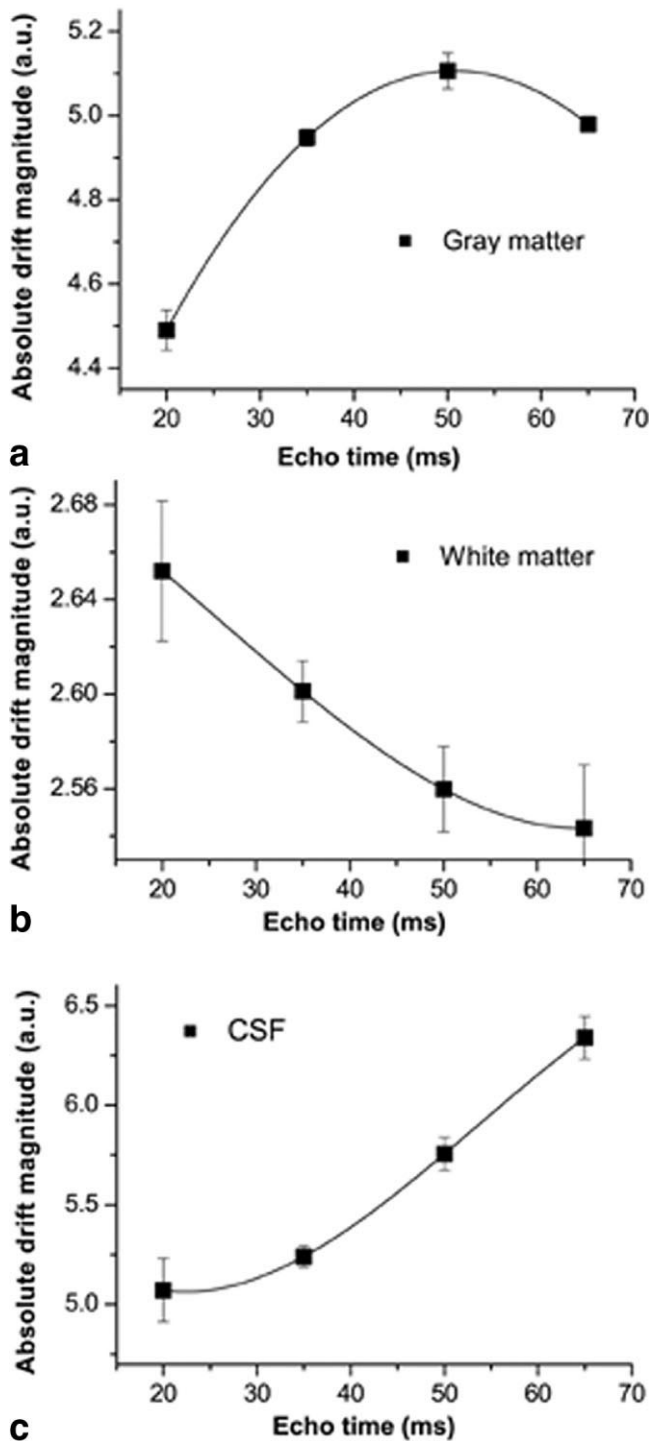
a

b

FIG. 3. Mean absolute drift magnitude as a function of TE in gray matter, white matter, and CSF ROIs acquired in seven human subjects. Error bars (± SEM) represent the variability across subjects.

FIG. 4. Mean absolute (a) and relative (b) magnitude of low-frequency drifts as a function of TE in agarose gel phantom. Error bars (± SEM) represent the variability across repeated measurements on the agarose gel phantom.

at longer TEs than shorter TEs (almost 1% for TE = 65 ms vs. approximately 0.2% for TE = 20 ms), suggesting an intrinsic link between baseline drift and task-induced activation in BOLD fMRI.

Within the activated ROI in visual cortex, we further found that the voxels showing greater task-induced BOLD signal changes exhibited greater magnitude of low-frequency drift at baseline. Figure 7a displays the scatter plot of baseline drift magnitudes vs. BOLD signal changes across activated pixels from a representative subject (all TEs are included). There was a strong positive association between the relative drift magnitude and fractional task-induced BOLD signal change across pixels in the visual ROI (r = 0.80, $P < 0.001$). This finding was so robust that statistical significance was reached for each of the seven subjects participating in the experiment at each of the four TEs (see Table 1 for representative TE of 35 ms).

Dependence of Low-Frequency Drift on Flip Angle

Figure 8 shows the mean relative drift magnitude as a function of flip angle in the whole brain averaged across eight human subjects (Fig. 8a) and an agarose phantom (Fig. 8b). In humans, the absolute magnitude of low-frequency drift increased with larger flip angle when the flip angle range was below the Ernst angle ($P < 0.01$), which can be translated into a positive dependence on the image intensity. Accordingly, the relative drift magnitude was largely insensitive to variations in flip angle ($P = 0.09$; see Fig. 8a) after the contribution of raw image intensity was removed. In contrast, such relationships were not observed in the agarose phantom (see Fig. 8b).

The representative time courses of BOLD fMRI data acquired with four different interleaved TEs were extracted from the visual area ROI and plotted in Fig. 6. As expected, the mean fractional signal change in response to visual stimulation was greater with prolonged TE. Interestingly, the baseline of BOLD signals also drifted to a greater extent
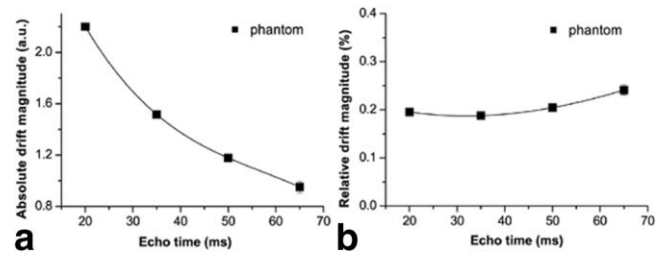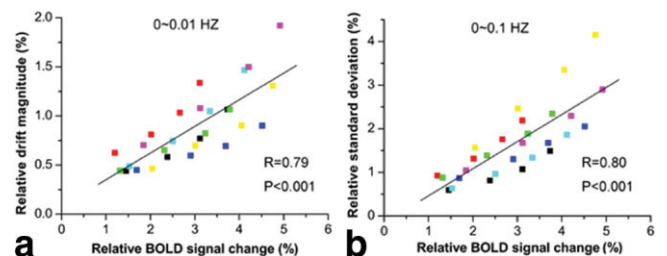

a

b

FIG. 5. Scatter plot of relative drift magnitudes (**a**) and spontaneous physiological fluctuations in the frequency band of 0.0–0.1 Hz (**b**) vs. relative BOLD signal changes in visual ROIs. Each color represents one subject.
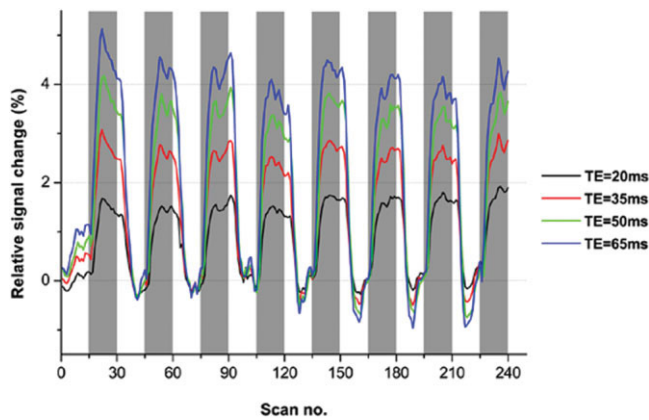
FIG. 6. The mean time courses of the fMRI scan with four inter-leaved TEs in the visual ROI averaged across seven subjects. The gray bars indicate time periods with visual stimulation.

Table 1
Linear Fitting Results (Model y = a + bx) Indicating Associations Between the Magnitude of Low Frequency Drifts and BOLD Signal Changes Across Pixels Within Activated Visual ROIs Using Dual-Echo EPI With Interleaved TE*

Subject	a	b	r
1	0.45	0.05	0.37[a]
2	0.56	0.12	0.44[a]
3	0.40	0.10	0.68[a]
4	0.46	0.04	0.32[a]
5	0.52	0.08	0.42[a]
6	0.64	0.13	0.67[a]
7	0.46	0.07	0.51[a]
Mean (SD)	0.50 (0.08)	0.08 (0.03)	

*Data with a representative TE of 35 ms are listed.
[a]Correlation is significant at the 0.01 level (two-tailed).

Drift Directions in Human Brain and Phantom

The drift direction was determined by comparing the ending and starting points of representative time courses of MRI scans. On average, the BOLD signal drifted upward $0.60 \pm 0.57\%$ ($P = 0.036$) during an 8-min resting scan in the whole brain of seven subjects, after correction of cardiac and respiratory pulsation effects. This trend was evident in the white matter ($0.58 \pm 0.36\%$, $P < 0.05$) and CSF ($0.91 \pm 0.62\%$, $P < 0.05$), but failed to reach statistical significance in the gray matter ($0.42 \pm 0.66\%$, $P = 0.14$). In phantom studies, the BOLD signal also drifted upward $0.61 \pm 0.29\%$ ($P = 0.024$) during an 8-min scan. The representative time courses in the phantom show a linear drift pattern, whereas the human time courses demonstrate larger variances and higher-order temporal structures (data not shown). These data suggest that drifts due to scanner instabilities may have a reproducible direction, while physiologic-related low-frequency fluctuations may add oscillation patterns that may compromise the drift direction (e.g., gray matter).

Relationship Between Drift and Low-Frequency Spontaneous Fluctuation of BOLD fMRI

It has been generally accepted that temporal components of BOLD fMRI series with frequency range <0.1Hz represent spontaneous fluctuations of metabolic-linked brain physiology (15,24,33,34), which can be utilized to characterize the resting state (e.g., connectivity analysis). To date, however, few studies have been dedicated to the understanding of the biophysical origin of slow drifts (0.00–0.01 Hz) as well as its role in spontaneous low-frequency fluctuations of BOLD fMRI. This is a potentially important issue since drifts (0.00–0.01 Hz) accounted for 38% of the energy (power) within the frequency band of 0.0–0.1 Hz, given only 10% of the spectral width. In the present study, we also compared the properties of signal fluctuations (determined by temporal SD) in different low-frequency bands of BOLD fMRI. We found that there was very similar dependence on TE in the two low-frequency bands of 0.00–0.01 Hz and 0.0–0.1 Hz (see Figs 2 and 9). Further analyses indicated that drifts accounted for 90.8% of the TE dependence of low-frequency fluctuations (0.0–0.1 Hz), whereas the fractional variations accounted for by the frequency band of 0.01–0.1 Hz was 96.1%.

As shown in Figs. 5 and 7, the low-frequency band of 0.0–0.1 Hz also demonstrated excellent (slightly stronger than drifts) correlation with visual cortex activation both across subjects and across pixels within individual subjects. Further analyses indicated that drifts accounted for 44% of variations of spontaneous low-frequency fluctuations (0.0–0.1 Hz) within activated visual cortex, whereas the fractional variations accounted for by the frequency band of 0.01–0.1 Hz was 82.5%. These data suggest that drift effects may be an important physiological component in spontaneous low-frequency fluctuations, with contributions comparable to the frequency band of 0.01–0.1 Hz.

DISCUSSION

To summarize the main findings from our study, we found that: 1) the spatial distribution of low-frequency drift was tissue-specific, with greater magnitude in the gray than in the white matter; 2) drifts in the human brain (especially
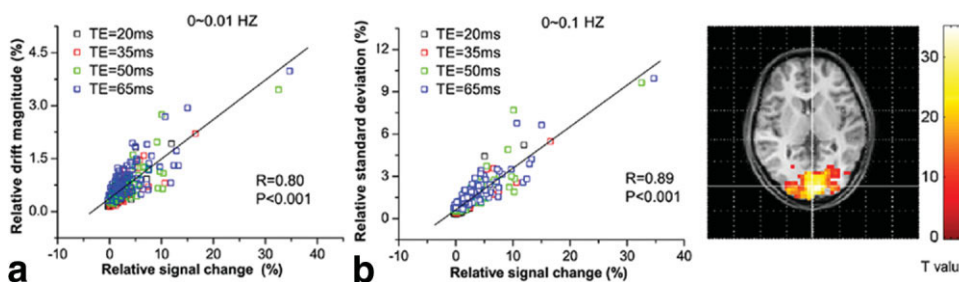

FIG. 7. Scatter plot of BOLD signal changes during activation vs. relative drift magnitudes (**a**) and spontaneous physiological fluctuations within 0.0–0.1 Hz across activated pixels in visual ROI. Data from a representative subject are shown and the visual ROI of this subject is displayed in the right column.
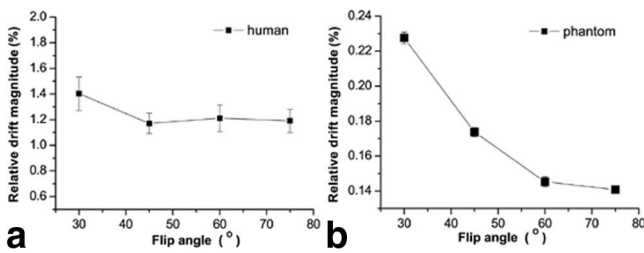
FIG. 8. Relative magnitude of low-frequency drifts as a function of flip angle in whole brain of eight human subjects (**a**) and agarose phantom (**b**). Error bars (± SEM) represent the variability across subjects as well as across multiple scans in phantom.

gray matter) presented characteristic dependence on TE that was similar to BOLD contrast (35) but different from those observed in the agarose phantom; and 3) there was a strong positive correlation between drift magnitudes at baseline and BOLD signal changes during task activation even on a pixel-by-pixel level. Compared to the reported spatiotemporal patterns of physiological noise in BOLD fMRI (16), our data suggest that fluctuations in brain metabolism and physiology may be the primary origin of low-frequency drift. As suggested by Krüger and Glover (16), spontaneous fluctuations in brain metabolism and physiology affect BOLD fMRI signals through two main mechanisms: temporal variations of T_2^* (ΔT_2^* effect) and fluctuations of raw image intensity (ΔM effect). The biophysical properties of the ΔT_2^* effect are identical to those underlying the BOLD contrast, which show that the absolute signal change reaches its maximum when TE equals T_2^*, and the relative signal change increases linearly with TE. The ΔM effect is simply a fraction of the raw image intensity. The overall physiological noise including both ΔT_2^* and ΔM effects still demonstrated the stereotypical TE dependence with the noise reaching its peak when TE approximated T_2^*. The relationships between magnitudes of low-frequency drift and imaging parameters such as TE and flip angle identified in our experiments are in excellent agreement with the findings of Krüger and Glover (16) as well as others (10,36).

In the present study, we also observed tissue-specific distribution of drift effects that are consistent with past studies on physiological noise in BOLD fMRI (16). In addition, the dependence of drift magnitudes on TE was different in gray matter, white matter, and CSF. Gray matter demonstrated the characteristic dependence on TE similar to that of the BOLD contrast, suggesting that neuronal activities in gray matter may be the main source of drift effects. In contrast, white matter not only manifested reduced drift magnitudes, the dependence on TE was also similar to that of an agarose phantom. This finding may suggest that white matter fibers do not contribute substantially to low-frequency fluctuations/drifts in BOLD fMRI. As a result, systemic and thermal noise may dominate low-frequency drifts in the white matter, thereby manifesting a pattern similar to that observed in phantom studies. Nevertheless, complete understanding of drift effects in different tissue types of human brain awaits further studies.

In the present study, elevated low-frequency noise was also present in phantom data. One argument to our claim

for physiological origin of low-frequency drift is that scanner instabilities may affect BOLD fMRI signals through similar mechanisms by causing temporal variations of T_2^* and image intensity (36). However, the relative magnitude of low-frequency drift in the phantom was approximately a quarter of that observed in human brain (see Figs. 2 and 4). Drift magnitude also exhibited contrasting dependencies on TE and flip angle between the agarose phantom and human brain. Our results are generally consistent with Smith et al. (9) showing the existence of drift effects in both inert phantom and human subjects. Nevertheless, our study expanded their findings by describing several aspects of the biophysical properties of drift effects, which demonstrated significant differences between human and phantom data. Using Eq. [4] of Ref. 16 to fit the mean absolute drift magnitudes in the present study, at TE = 35 ms, thermal and MR system noise accounted for approximately 25% of drift effects, while ΔT_2^* and ΔM effects accounted for approximately 61% and 14% of slow drifts, respectively. Our data suggest that low-frequency drifts in BOLD fMRI are likely to reflect a combination of physiological noise and scanner instabilities, with a ratio of approximately 3:1.

Physiological noise may arise from systemic sources such as cardiac and respiratory cycles, in addition to spontaneous neuronal events. Cardiac and respiratory pulsations may contribute to low-frequency noise through aliasing, especially for the effective TR of 2 s (19). In our study, we removed respiratory and cardiac effects through image-based retrospective correction. Figure 2 showed the contribution of cardiac and respiratory effects in low-frequency drifts (21,22) with an effective TR of 2 s, which accounted for approximately 4.4% of the absolute drift magnitude in the whole brain. As shown in Fig. 2, the respiratory and cardiac effects have little influence on the relationship between drift magnitudes and TE. Additionally, to further verify our findings, we adopted a short effective TR of 250 ms that was unlikely to be affected by aliasing effects. These experiments provided convergent evidence that the dependence of drifts on TE was not caused by aliasing of cardiac and respiratory pulsations.

An important fMRI modality related to drift effects is the interregional correlations of spontaneous low-frequency fluctuations in BOLD fMRI (<0.1 Hz), often referred to as "functional connectivity." In a few early studies, functional connectivity was considered to exist within the frequency band of less than 0.1 Hz or 0.08 Hz (11,12). However, in many of the later studies on functional con-
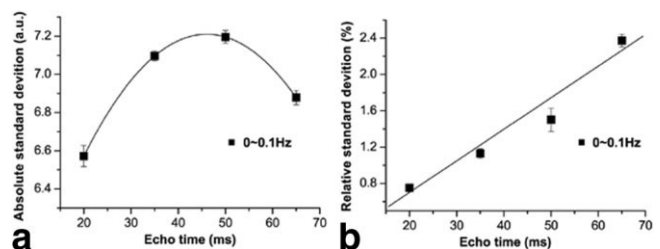

FIG. 9. Mean absolute (a) and relative SD (b) of low-frequency physiological noise (<0.1 Hz) as a function of TE in the whole brain acquired in seven human subjects.

nectivity, low-frequency drifts below 0.01 Hz were considered to be scanner-related and were generally removed or corrected for (13,15). These different treatments of slow drifts in connectivity analyses reflect controversies in current understandings of the underlying biophysical mechanism. One of the main goals of the present study was to address this ambiguity regarding drift effects in BOLD fMRI. We found that drifts accounted for a relative large portion of the physiological fluctuations between 0 and 0.1 Hz, given only 1/10 of the spectral width. Both the dependence on TE and the relationship with task-induced BOLD signal changes were very similar between the low-frequency bands of 0.00−0.01 Hz and 0.0−0.1 Hz. In addition, we performed connectivity analyses using resting state BOLD fMRI data within the frequency band of 0.01−0.1 Hz and 0.00−0.01 Hz, respectively. The frequency band of 0.01−0.1 Hz demonstrated clear functional connectivity in the motor cortex, while the low-frequency drift showed more global correlations within the whole cortex. Despite evidence supporting the origin of spontaneous fluctuations, whether low-frequency drifts contribute to interregional connectivity is a question that merits further research.

The strong correlations between drift magnitude at baseline and task-induced BOLD signal change across pixels match well with Hyde et al. (10), suggesting that baseline drifts and BOLD fMRI signals are governed by the same or similar metabolic and physiologic mechanisms. This observation prompts the hypothesis that the magnitude of low-frequency drift at baseline in each brain pixel may represent the "susceptibility" of that pixel to perturbations of oxygen-sensitive MRI signals. Therefore, brain pixels displaying greater drifts at baseline because of its high sensitivity to spontaneous fluctuations in metabolic-linked brain physiology will show greater BOLD signal change in the event of increased blood flow response to neuronal activation. If the above hypothesis were true, it might have several implications. Despite the success of BOLD fMRI in visualizing regional brain activation to sensorimotor and cognitive tasks, there remain few effective approaches to quantify the "resting state" in BOLD fMRI (24). Functional connectivity has been widely validated but limited to specific brain regions related to sensorimotor, language, and attention functions. As demonstrated in the present study, if the low-frequency drift in the brain parenchyma arises primarily from spontaneous neuronal events, it may offer a potentially valuable physiologic and metabolic index of baseline brain function. In patient populations that are not suitable for task-activation studies (e.g., stroke, dementia), drift magnitudes measured at baseline may provide a surrogate index of neuronal function without performing specific tasks (37). Another shortcoming of the BOLD contrast is that it relies on a complex interplay between cerebral blood flow, blood volume, and oxygen metabolism, as well as other biophysical parameters, often resulting in large intersubject variability of BOLD fMRI signals (7). Low-frequency drifts at baseline may be used as a reference to calibrate fMRI signals during task activation to improve the test-retest repeatability and intersubject variability of BOLD fMRI. For instance, the magnitude of baseline drifts can be included as a covariate in group GLM analysis to account for intersubject varia-

tions in task-induced BOLD signal changes (given that drifts are correlated with fMRI signals across subjects).

One interesting argument raised in the fMRI community is the benefit for BOLD fMRI at high and ultrahigh fields. This argument is based on the observation that at high and ultrahigh fields, physiological noise will become the dominating source of temporal fluctuations in BOLD fMRI (38). Because physiological noise is magnified at high fields, there may be little benefit for performing BOLD fMRI above 4T. Based on the present study, low-frequency fluctuations and drifts in baseline BOLD fMRI data may reflect spontaneous fluctuations of brain physiology and metabolism, and may to a certain degree predict the BOLD response to task activation. High and ultrahigh magnets may be ideal for resting state studies given the increased drift effects and physiological noise of BOLD fMRI.

CONCLUSION

In the present work, we investigated the biophysical mechanism of low-frequency drift in BOLD fMRI by considering three main sources of signal variations including scanner instabilities, cardiac and respiratory pulsations, and spontaneous fluctuations of metabolic-linked brain physiology. Drift effects in human brain, especially within the gray matter, were found to mainly reflect spontaneous fluctuations of brain metabolism and physiology. These findings corroborated and extended existing studies on biophysical mechanisms underlying low-frequency fluctuations in BOLD fMRI, and may have several implications for quantifying and standardizing the BOLD contrast for future fMRI studies.

REFERENCES

1. Bandettini PA, Jesmanowicz A, Wong EC, Hyde JS. Processing strategies for time-course data sets in functional MRI of the human brain. Magn Reson Med 1993;30:161–173.
2. Bullmore E, Brammer M, Williams SC, Rabe-Hesketh S, Janot N, David A, Mellers J, Howard R, Sham P. Statistical methods of estimation and inference for functional MR image analysis. Magn Reson Med 1996;35: 261–277.
3. Mattay VS, Frank JA, Santha AK, Pekar JJ, Duyn JH, McLaughlin AC, Weinberger DR. Whole-brain functional mapping with isotropic MR imaging. Radiology 1996;201:399–404.
4. Zarahn E, Aguirre GK, D'Esposito M. Empirical analyses of BOLD fMRI statistics. I. Spatially unsmoothed data collected under null-hypothesis conditions. Neuroimage 1997;5:179–197.
5. Friston KJ, Josephs O, Zarahn E, Holmes AP, Rouquette S, Poline J. To smooth or not to smooth? Bias and efficiency in fMRI time-series analysis. Neuroimage 2000;12:196–208.
6. Purdon PL, Weisskoff RM. Effect of temporal autocorrelation due to physiological noise and stimulus paradigm on voxel-level false-positive rates in fMRI. Hum Brain Mapp 1998;6:239–249.
7. Aguirre GK, Detre JA, Zarahn E, Alsop DC. Experimental design and the relative sensitivity of BOLD and perfusion fMRI. Neuroimage 2002;15: 488–500.
8. Wang J, Aguirre GK, Kimberg DY, Roc AC, Li L, Detre JA. Arterial spin labeling perfusion fMRI with very low task frequency. Magn Reson Med 2003;49:796–802.

9. Smith AM, Lewis BK, Ruttimann UE, Ye FQ, Sinnwell TM, Yang Y, Duyn JH, Frank JA. Investigation of low frequency drift in fMRI signal. Neuroimage 1999;9:526−533.

10. Hyde JS, Biswal BB, Jesmanowicz A. High-resolution fMRI using multislice partial k-space GR-EPI with cubic voxels. Magn Reson Med 2001;46:114−125.

11. Biswal B, Yetkin FZ, Haughton VM, Hyde JS. Functional connectivity in the motor cortex of resting human brain using echo-planar MRI. Magn Reson Med 1995;34:537−541.

12. Lowe MJ, Mock BJ, Sorenson JA. Functional connectivity in single and multislice echoplanar imaging using resting-state fluctuations. Neuroimage 1998;7:119−132.

13. Peltier SJ, Noll DC. T(2)(*) dependence of low frequency functional connectivity. Neuroimage 2002;16:985−992.

14. Greicius MD, Krasnow B, Reiss AL, Menon V. Functional connectivity in the resting brain: a network analysis of the default mode hypothesis. Proc Natl Acad Sci USA 2003;100:253−258.

15. Fransson P. Spontaneous low-frequency BOLD signal fluctuations: an fMRI investigation of the resting-state default mode of brain function hypothesis. Hum Brain Mapp 2005;26:15−29.

16. Kruger G, Glover GH. Physiological noise in oxygenation-sensitive magnetic resonance imaging. Magn Reson Med 2001;46:631−637.

17. Bhattacharyya PK, Lowe MJ. Cardiac-induced physiologic noise in tissue is a direct observation of cardiac-induced fluctuations. Magn Reson Imaging 2004;22:9−13.

18. Shmueli K, van Gelderen P, de Zwart JA, Horovitz SG, Fukunaga M, Jansma JM, Duyn JH. Low-frequency fluctuations in the cardiac rate as a source of variance in the resting-state fMRI BOLD signal. Neuroimage 2007;38:306−320.

19. Frank LR, Buxton RB, Wong EC. Estimation of respiration-induced noise fluctuations from undersampled multislice fMRI data. Magn Reson Med 2001;45:635−644.

20. Kiviniemi V, Ruohonen J, Tervonen O. Separation of physiological very low frequency fluctuation from aliasing by switched sampling interval fMRI scans. Magn Reson Imaging 2005;23:41−46.

21. Dagli MS, Ingeholm JE, Haxby JV. Localization of cardiac-induced signal change in fMRI. Neuroimage 1999;9:407−415.

22. Birn RM, Diamond JB, Smith MA, Bandettini PA. Separating respiratory-variation-related fluctuations from neuronal-activity-related fluctuations in fMRI. Neuroimage 2006;31:1536−1548.

23. Peltier SJ, Noll DC. Analysis of fMRI signal and noise component TE dependence. Neuroimage 2000;11(5 Suppl 1):S623.

24. Fox MD, Raichle ME. Spontaneous fluctuations in brain activity observed with functional magnetic resonance imaging. Nat Rev 2007;8:700−711.

25. Mitchell MD, Kundel HL, Axel L, Joseph PM. Agarose as a tissue equivalent phantom material for NMR imaging. Magn Reson Imaging 1986;4:263−266.

26. Aguirre GK, Zarahn E, D'Esposito M. Empirical analyses of BOLD fMRI statistics. II. Spatially smoothed data collected under null-hypothesis and experimental conditions. Neuroimage 1997;5:199−212.

27. Wang J, Wang Z, Aguirre GK, Detre JA. To smooth or not to smooth? ROC analysis of perfusion fMRI data. Magn Reson Imaging 2005;23:75−81.

28. Glover GH, Li TQ, Ress D. Image-based method for retrospective correction of physiological motion effects in fMRI: RETROICOR. Magn Reson Med 2000;44:162−167.

29. Speck O, Hennig J. Functional imaging by I0- and T2*-parameter mapping using multi-image EPI. Magn Reson Med 1998;40:243−248.

30. Wansapura JP, Holland SK, Dunn RS, Ball WS, Jr. NMR relaxation times in the human brain at 3.0 Tesla. J Magn Reson Imaging 1999;9:531−538.

31. Peran P, Hagberg G, Luccichenti G, Cherubini A, Brainovich V, Celsis P, Caltagirone C, Sabatini U. Voxel-based analysis of R2* maps in the healthy human brain. J Magn Reson Imaging 2007;26:1413−1420.

32. Kruger G, Kastrup A, Glover GH. Neuroimaging at 1.5 T and 3.0 T: comparison of oxygenation-sensitive magnetic resonance imaging. Magn Reson Med 2001;45:595−604.

33. Cordes D, Haughton VM, Arfanakis K, Carew JD, Turski PA, Moritz CH, Quigley MA, Meyerand ME. Frequencies contributing to functional connectivity in the cerebral cortex in "resting-state" data. AJNR Am J Neuroradiol 2001;22:1326−1333.

34. Cordes D, Haughton VM, Arfanakis K, Wendt GJ, Turski PA, Moritz CH, Quigley MA, Meyerand ME. Mapping functionally related regions of brain with functional connectivity MR imaging. AJNR Am J Neuroradiol 2000;21:1636−1644.

35. Menon RS, Ogawa S, Tank DW, Ugurbil K. Tesla gradient recalled echo characteristics of photic stimulation-induced signal changes in the human primary visual cortex. Magn Reson Med 1993;30:380−386.

36. Wu G, Li SJ. Theoretical noise model for oxygenation-sensitive magnetic resonance imaging. Magn Reson Med 2005;53:1046−1054.

37. Wang HH, Menezes NM, Zhu MW, Ay H, Koroshetz WJ, Aronen HJ, Karonen JO, Liu Y, Nuutinen J, Wald LL, Sorensen AG. Physiological noise in MR images: an indicator of the tissue response to ischemia? J Magn Reson Imaging 2008;27:866−871.

38. Triantafyllou C, Hoge RD, Krueger G, Wiggins CJ, Potthast A, Wiggins GC, Wald LL. Comparison of physiological noise at 1.5 T, 3 T and 7 T and optimization of fMRI acquisition parameters. Neuroimage 2005;26:243−250.